Mechanistic Investigation of the Electrochemical Reduction of Cp_2TiX_2

Rasmus Juel Enemærke, Jens Larsen, Troels Skrydstrup, and Kim Daasbjerg*

Department of Chemistry, University of Aarhus, Langelandsgade 140, 8000 Aarhus C, Denmark

Received December 11, 2003

The mechanism for the electrochemical reduction of titanocene dihalides, Cp_2TiX_2 (X = Cl, Br, I), in tetrahydrofuran has been described successfully using a common mesh scheme. On the basis of simulations of recorded cyclic voltammograms it has been possible to evaluate a number of thermodynamic and kinetic parameters for the species involved: i.e., $Cp_2TiX_2^-$, $(Cp_2TiX)_2$, Cp_2TiX, and Cp_2Ti^+. In general, the standard potentials of the oxidized titanium-based species increase (i.e. become less negative) in the orders Cp_2TiX_2, $(Cp_2TiX)_2^+$, Cp_2TiX^+, $CpTi^{2+}$ and X = Cl, Br, I. From the extracted data pertaining to electrochemically reduced solutions of Cp_2TiX_2, it becomes evident that while $Cp_2TiX_2^-$ is the major constituent for X = Cl, Cp_2TiX and $(Cp_2TiX)_2$ are the main species in the cases of X = Br, I. The presence of $(Cp_2TiX)_2$ is surprising, as the solvent tetrahydrofuran was believed to be capable of breaking the weak dimeric structure. Kinetic investigations of the reactions between electrochemically reduced solutions of Cp_2TiX_2 and benzyl chloride show that the reactive species are Cp_2TiX and $(Cp_2TiX)_2$, with almost no contribution from $Cp_2TiX_2^-$, even in the case of X = Cl.

Introduction

Single-electron-transferring agents based on low-valent transition-metal complexes have demonstrated a significant utility for a variety of organic synthetic transformations.[1−9] An important representative of these complexes is the Ti^{III} species bis(cyclopentadienyl)titanium chloride (Cp_2TiCl), which has developed into a popular reagent for promoting regioselective epoxide openings to alkyl radicals and highly diastereoselective pinacol couplings as well as halide reductions.[6−9] Various methods exist for the preparation of this reagent, including the coupling of metalated cyclopentadiene with $TiCl_3$[10] and the facile reduction of the Ti^{IV} complex Cp_2TiCl_2 with metals such as zinc,[11] aluminum,[12] and manganese.[13]

In this paper we wish to consider the prospects of using an electrochemical rather than chemical approach in the reduction of Cp_2TiX_2 (X = Cl, Br, I), as this might prove to be a convenient route for generating Ti^{III}-based species without the need of metal reductants. Another aim is to describe in detail the mechanism for the reduction of Cp_2TiX_2 on the basis of cyclic voltammetric and kinetic measurements, in order to elucidate the nature of the different species present in solution. At the same time we will attempt to extract quantitative information from the recorded voltammograms by employing digital simulations and settle a longstanding dispute concerning whether $Cp_2TiCl_2^-$ produced from the reduction of Cp_2TiCl_2 is stable[14−16] or dissociates to give Cp_2TiCl and Cl^-.[17,18] Previous electrochemical investigations have been carried out by means of polarography[19−23] and cyclic voltammetry[14−18,24−29] in various solvents such as *N*,*N*-dimethylformamide, for-

* To whom correspondence should be addressed. E-mail: kdaa@chem.au.dk. Fax: +45 86196199.

(1) Molander, G. A.; Harris, C. R. *Chem. Rev.* **1996**, *96*, 307.
(2) Molander, G. A.; Harris, C. R. *Tetrahedron* **1998**, *54*, 3321.
(3) Skrydstrup, T. *Angew. Chem., Int. Ed. Engl.* **1997**, *36*, 345.
(4) Krief, A.; Laval, A.-M. *Chem. Rev.* **1999**, *99*, 745.
(5) Steel, P. G. *J. Chem. Soc., Perkin Trans. 1* **2001**, 2727.
(6) Gansäuer, A.; Bluhm, H. *Chem. Rev.* **2000**, *100*, 2771.
(7) Gansäuer, A. In *Radicals in Organic Synthesis*; Renaud, P., Sibi, M. P., Eds.; Wiley-VCH: Weinheim, Germany, 2001; Vol. 2, p 2007.
(8) Gansäuer, A.; Lauterbach, T.; Narayan, S. *Angew. Chem., Int. Ed.* **2003**, *42*, 5556.
(9) Spencer, R. P.; Schwartz, J. *Tetrahedron* **2000**, *56*, 2103.
(10) Manzer, L. E. *Inorg. Synth.* **1982**, *21*, 84.
(11) Coutts, R. S. P.; Wailes, P. C.; Martin, R. L. *J. Organomet. Chem.* **1973**, *47*, 375.
(12) Birmingham, J. M.; Fischer, A. K.; Wilkinson, G. *Naturwissenschaften* **1955**, *42*, 96.
(13) Sekutowski, D. G.; Stucky, G. D. *Inorg. Chem.* **1975**, *14*, 2192.
(14) El Murr, N.; Chaloyard, A.; Tirouflet, J. *J. Chem. Soc., Chem. Commun.* **1980**, 446.
(15) Johnston, R. F.; Borjas, R. E.; Furilla, J. L. *Electrochim. Acta* **1995**, *40*, 473.
(16) Langmaier, J.; Samec, Z.; Varga, V.; Horáček, M.; Mach, K. *J. Organomet. Chem.* **1999**, *579*, 348.
(17) Mugnier, Y.; Moise, C.; Laviron, E. *J. Organomet. Chem.* **1981**, *210*, 69.
(18) Meunier-Prest, R.; Lamblin, G.; Mailfert, A.; Raveau, M. S. *J. Electroanal. Chem.* **2003**, *541*, 175.
(19) Hsiung, H.; Brown, G. H. *J. Electrochem. Soc.* **1963**, *110*, 1085.
(20) Dessy, R. E.; King, R. B.; Waldrop, M. *J. Am. Chem. Soc.* **1966**, *88*, 5112.
(21) Valcher, S.; Mastragostino, M. *J. Electroanal. Chem. Interfacial Electrochem.* **1967**, *14*, 219.
(22) Gubin, S. P.; Smirnova, S. A. *J. Organomet. Chem.* **1969**, *20*, 229.
(23) Laviron, E.; Besançon, J.; Huq, F. *J. Organomet. Chem.* **1978**, *159*, 279.
(24) Mugnier, Y.; Moise, C.; Laviron, E. *J. Organomet. Chem.* **1981**, *204*, 61.
(25) El Murr, N.; Chaloyard, A. *J. Organomet. Chem.* **1981**, *212*, C39.
(26) El Murr, N.; Chaloyard, A. *J. Organomet. Chem.* **1982**, *231*, 1.
(27) Mugnier, Y.; Moïse, C.; Laviron, E. *Nouv. J. Chim.* **1982**, *6*, 197.
(28) Mugnier, Y.; Fakhr, A.; Fauconet, M.; Moise, C.; Laviron, E. *Acta Chem. Scand.* **1983**, *B27*, 423.
(29) Samuel, E.; Vedel, J. *Organometallics* **1989**, *8*, 237.

10.1021/om034360h CCC: $27.50
Publication on Web 03/12/2004

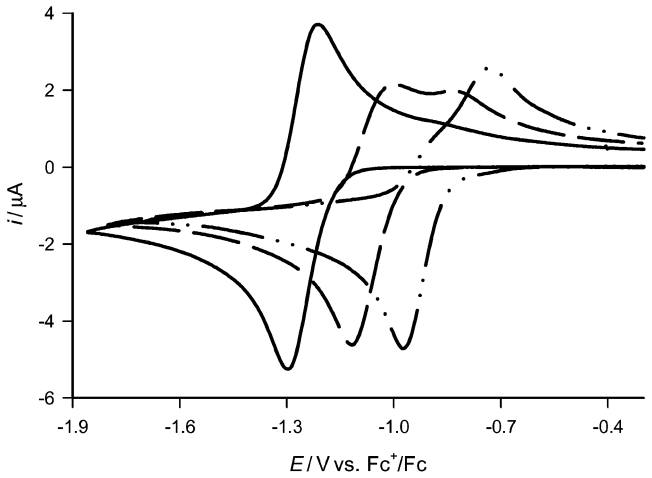

Figure 1. Cyclic voltammograms of 1 mM Cp_2TiCl_2 (—), Cp_2TiBr_2 (– –) and Cp_2TiI_2 (– ·· –) recorded at a sweep rate of 1 V s^{-1} in 0.2 M Bu_4NPF_6/THF.

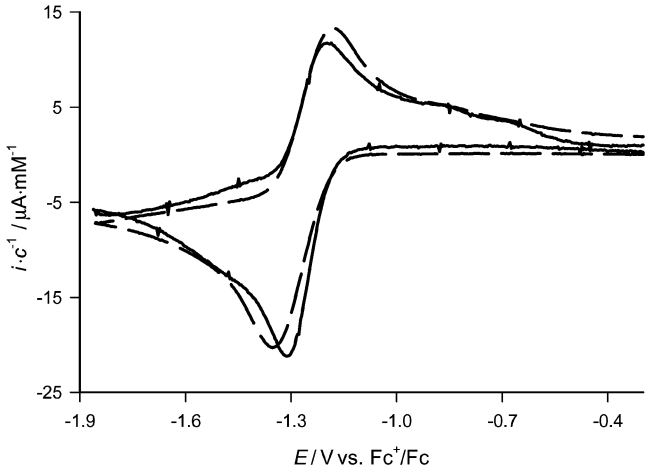

Figure 2. Cyclic voltammograms of Cp_2TiCl_2 in concentrations of 0.4 (—) and 2.0 mM (– –) recorded at a sweep rate of 20 V s^{-1} in 0.2 M Bu_4NPF_6/THF. Currents are normalized with respect to concentration.

mamide, and tetrahydrofuran (THF). Because THF is the solvent most commonly used for the chemical reactions involving Ti^{III} complexes, we have selected it for our study.

Results and Discussion

Typical cyclic voltammograms of Cp_2TiX_2 (X = Cl, Br, I) recorded at a sweep rate of 1 V s^{-1} are collected in Figure 1. Apparently, these voltammograms show that the degree of chemical reversibility decreases as the halogen is changed from Cl to Br and I. In a first approach, we will base our interpretation on an E_qC_r reaction scheme as proposed originally by Laviron et al. for Cp_2TiCl_2.[17] This mechanism is depicted in eqs 1 and 2, where the quasi-reversible electrochemical reduction of Cp_2TiX_2 is followed by a fast and chemically reversible cleavage of $Cp_2TiX_2^-$. Within this scheme the

$$Cp_2TiX_2 + e^- \rightleftarrows Cp_2TiX_2^- \quad (1)$$

$$Cp_2TiX_2^- \underset{k_{-2}}{\overset{k_2}{\rightleftharpoons}} Cp_2TiX + X^- \quad (2)$$

different oxidation wave patterns observed in the voltammograms would simply be ascribed to differences in the rate constants k_2 and k_{-2}. While $Cp_2TiCl_2^-$ is the species detectable on the reverse sweep for X = Cl with no apparent influence from the cleavage reaction, another species besides $Cp_2TiBr_2^-$ is clearly formed upon reducing Cp_2TiBr_2. This new species, tentatively assigned to Cp_2TiBr, is formed following the cleavage of Br^- from $Cp_2TiBr_2^-$. In the case of Cp_2TiI_2 the influence from the cleavage reaction is even more pronounced, in the sense that the wave pertaining to $Cp_2TiI_2^-$ is completely absent and replaced by that of Cp_2TiI.

The means available in our hands for elucidating the mechanism in cyclic voltammetry are related to the recording of the current response upon changing experimental parameters such as concentration and sweep rate. For instance, an increase in the concentration of X^- or Cp_2TiX_2 should favor the second-order back-association reaction of eq 2, thus making the oxidation wave of $Cp_2TiX_2^-$ more pronounced on the reverse sweep. Note that for an E_qC_i mechanism, in which the chemical step is irreversible, there would be no such dependency. As to the effect of increasing the sweep rate, the expectation is that the $Cp_2TiX_2^-$ oxidation wave should decrease relative to the subsequent wave on the assumption that the equilibrium reactions in eqs 1 and 2 both are relatively fast. This is related to the fact that eq 2 will have less time for responding to the consumption of $Cp_2TiX_2^-$ in the oxidation process of eq 1. If sufficiently high sweep rates are applied, one may attain the situation where the back-association reaction of eq 2 is completely outrun and cannot feed eq 1 with $Cp_2TiX_2^-$ any longer. In this domain, the system behaves like an E_qC_i mechanism, in which the kinetic control is mainly by the forward cleavage reaction and no $Cp_2TiX_2^-$ oxidation wave can be observed. Ultimately, even the cleavage reaction may be outrun, thus leaving the electrode process in eq 1 as the only essential reaction, as envisioned by the reappearance of the oxidation wave of $Cp_2TiX_2^-$. At the same time, the quasi-reversible nature of the electrode process will show up as an increase of the peak separation.

Cp_2TiCl_2 (Part I). Cyclic voltammograms of Cp_2TiCl_2 recorded at a high sweep rate of 20 V s^{-1} at two different concentrations are shown in Figure 2. The presence of the $Cp_2TiCl_2/Cp_2TiCl_2^-$ wave is the most characteristic feature of these voltammograms, although a closer inspection reveals that possibly two other small oxidation waves are detectable in the range from −0.9 to −0.6 V vs Fc^+/Fc (abbreviation for ferrocenium/ferrocene). The fact that the relatively largest contribution from the latter waves is found at the lowest concentrations and the largest sweep rates employed (see Figure 1 for a comparison) is consistent with the E_qC_r rather than the E_qC_i mechanism as discussed above. Moreover, as seen in Figure 3, addition of Bu_4NCl to the solution results in their complete disappearance because of the shift in the equilibrium reaction of eq 2 toward the left. A shift in the opposite direction can be accomplished through addition of an electron-donating cosolvent such as hexamethylphosphoramide (HMPA), which has a profound ability of coordinating as a ligand to metal nuclei.[30] As shown in Figure 3, the $Cp_2TiCl_2^-$ oxidation

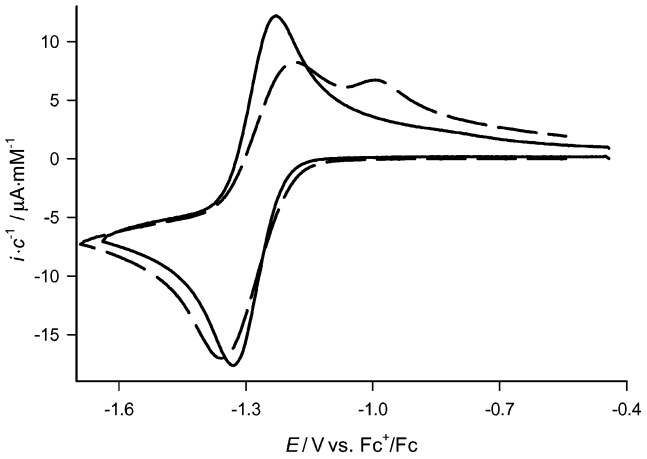

Figure 3. Cyclic voltammograms of 0.75 mM Cp_2TiCl_2 in the presence of 10 mM Bu_4NCl (—) and 2.5 mM Cp_2TiCl_2 in the presence of 25 mM HMPA (— —) recorded at a sweep rate of 10 V s^{-1} in 0.2 M Bu_4NPF_6/THF. Currents are normalized with respect to concentration.

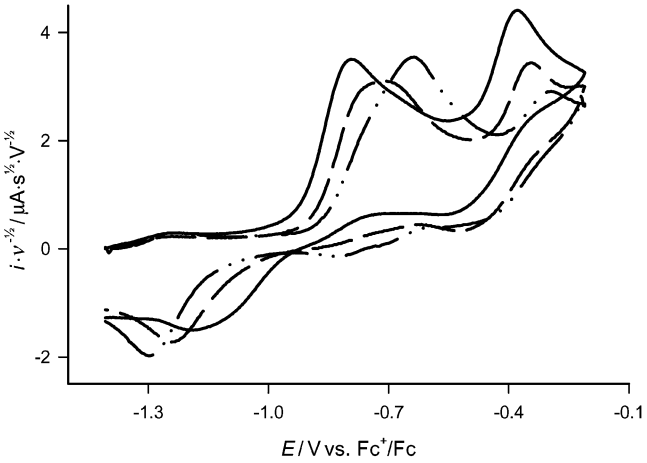

Figure 4. Cyclic voltammograms of 1.5 mM "Cp_2TiCl" recorded at sweep rates of 0.1 (—), 1 (— —), and 10 V s^{-1} (— ·· —) in 0.2 M Bu_4NPF_6/THF. Currents are normalized with respect to sweep rate.

wave diminishes at the expense of a new wave at −1.0 V vs Fc^+/Fc, assigned to the HMPA-coordinated Cp_2TiCl species.

"Cp_2TiCl". With the aim of identifying the cleavage product(s) formed in eq 2, a presumed solution of Cp_2TiCl was prepared in THF by reacting $TiCl_3$ with 2 equiv of TlCp (see the Experimental Section). In the following, this solution will be denoted "Cp_2TiCl", since it turned out that Cp_2TiCl was not the only species present. Cyclic voltammograms of "Cp_2TiCl" recorded at different sweep rates and concentrations are depicted in Figures 4 and 5.

Laviron et al.[17] suggested that the first broad oxidation wave at −0.8 V vs Fc^+/Fc should be assigned to the oxidation of Cp_2TiCl depicted in eq 3. The wave at −0.4

$$Cp_2TiX - e \rightleftarrows Cp_2TiX^+ \qquad (3)$$

V vs Fc^+/Fc was attributed to the oxidation of the cation Cp_2Ti^+ (eq 4), generated during the sweep in a so-called

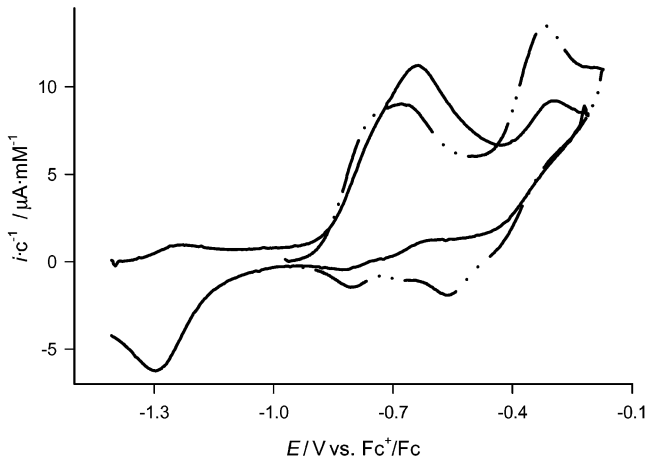

Figure 5. Cyclic voltammograms of "Cp_2TiCl" in concentrations of 1 (—) and 2.5 mM (— ·· —) recorded at a sweep rate of 10 V s^{-1} in 0.2 M Bu_4NPF_6/THF. Currents are normalized with respect to concentration.

father−son reaction, as shown in eq 5.[17] Indeed, the

$$Cp_2Ti^+ - e \rightleftarrows Cp_2Ti^{2+} \qquad (4)$$

$$Cp_2TiX + Cp_2TiX^+ \underset{k_{-5}}{\overset{k_5}{\rightleftharpoons}} Cp_2Ti^+ + Cp_2TiX_2 \qquad (5)$$

observations that the reduction of Cp_2TiCl_2 can be detected on the reverse sweep and that there is a decrease in the normalized oxidation current of Cp_2Ti^+ upon increasing the sweep rate or lowering the substrate concentration are in accordance with the presence of eq 5. Moreover, a cyclic voltammogram recorded on an authentic sample of the salt Cp_2TiPF_6 shows a wave at the expected potential of −0.4 V vs Fc^+/Fc.[31] On the other hand, the increase of the normalized reduction current of the Cp_2TiCl_2 wave as a function of sweep rate cannot be encompassed adequately within this picture (see the Supporting Information for further discussion of this point).

Although the above reaction scheme seems quite consistent with the experimental features, a closer inspection of the wave appearing at −0.8 V vs Fc^+/Fc reveals that the mechanism is more complex than originally proposed. Actually, this broad wave consists of two peaks, where the first one becomes more dominant as the sweep rate decreases and the concentration increases as shown in Figures 4 and 5, respectively. On this basis, we propose that the first peak should be attributed to the oxidation of the dimeric $(Cp_2TiCl)_2$ species (eq 6) and the second one to the oxidation of Cp_2TiCl (eq 3), with their relative heights being affected by the equilibrium reaction depicted in eq 7.

$$(Cp_2TiX)_2 - e \rightleftarrows (Cp_2TiX)_2^+ \qquad (6)$$

$$2Cp_2TiX \underset{k_{-7}}{\overset{k_7}{\rightleftharpoons}} (Cp_2TiX)_2 \qquad (7)$$

The $(Cp_2TiCl)_2$ dimer is known from the solid state[32] (see Chart 1), but its presence in solution is surprising,

(30) Enemærke, R. J.; Hertz, T.; Skrydstrup, T.; Daasbjerg, K. *Chem. Eur. J.* **2000**, *6*, 3747.

(31) Enemærke, R. J.; Larsen, J.; Skrydstrup, T.; Daasbjerg, K. Submitted for publication.

(32) Coutts, R. S. P.; Wailes, P. C.; Martin, R. L. *J. Organomet. Chem.* **1973**, 375.

Chart 1. Proposed Structure of the $(Cp_2TiCl)_2$ Dimer[32]

$(Cp_2TiCl)_2$ =

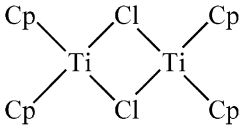

as THF was believed to be capable of breaking the weak structure.[29,33] The possibility that the dimer actually is of a half-open type, in which one of the bridges is broken, cannot be excluded, as discussed elsewhere.[31] Another interesting point is that eqs 3 and 5, involving the oxidation of Cp_2TiCl followed by the father−son reaction, cannot be the only pathway for the generation of Cp_2Ti^+ during the cyclic voltammetric sweep. The Cp_2Ti^+ peak is also apparent at high concentrations, although the oxidation goes almost exclusively through $(Cp_2TiCl)_2$ in eq 6 under such conditions. This implies that Cp_2Ti^+ may originate from the fragmentation of $(Cp_2TiCl)_2^+$ as well. On account of the observations that the reduction of Cp_2TiCl_2 is detectable on the reverse sweep and that the peak current ratio for the oxidation waves of $(Cp_2TiCl)_2$ and Cp_2Ti^+ approaches unity at low sweep rates, the fragmentation is proposed to follow the pathway shown in eq 8.

$$(Cp_2TiX)_2^+ \underset{k_{-8}}{\overset{k_8}{\rightleftharpoons}} Cp_2Ti^+ + Cp_2TiX_2 \qquad (8)$$

Cp_2TiCl_2 (Part II). Returning to the voltammograms of Cp_2TiCl_2 presented in Figure 2, it is suggested on the basis of the above analysis of "Cp_2TiCl" that the two small waves observed in the range from −0.9 to −0.6 V vs Fc^+/Fc should be attributed to the oxidation processes of $(Cp_2TiCl)_2$ and Cp_2TiCl, respectively. The noteworthy absence of the Cp_2Ti^+ wave is due to the fact that chloride liberated from the cleavage of $Cp_2TiCl_2^-$ in eq 2 will react with Cp_2TiCl^+ and $(Cp_2TiCl)_2^+$; i.e., eqs 5 and 8 should be replaced in this case by eqs 9 and 10.

$$Cp_2TiX^+ + X^- \underset{k_{-9}}{\overset{k_9}{\rightleftharpoons}} Cp_2TiX_2 \qquad (9)$$

$$(Cp_2TiX)_2^+ + X^- \underset{k_{-10}}{\overset{k_{10}}{\rightleftharpoons}} Cp_2TiX + Cp_2TiX_2 \qquad (10)$$

Cp_2TiBr_2. Cyclic voltammograms of Cp_2TiBr_2 recorded for different concentrations and sweep rates are collected in Figures 6 and 7. The overall picture emerging is in line with that for Cp_2TiCl_2, in that the wave for the $Cp_2TiBr_2/Cp_2TiBr_2^-$ redox couple becomes more pronounced at high concentrations, at low sweep rates, and in particular in the presence of Bu_4NBr (see inset of Figure 6), due to a profound shift of the reversible cleavage reaction in eq 2 toward the left. Still, the characterization of eq 2 is much more straightforward in this case, as the oxidation peaks assigned to the cleavage products are substantially larger. For voltammograms recorded at high sweep rates and low concentrations (see the Supporting Information), it is evident that the broad wave appearing at −0.8 V vs Fc^+/Fc involves two processes attributed to the oxidations of $(Cp_2TiBr)_2$ and Cp_2TiBr and that the relative contribution of the former becomes larger as the concentration is raised. The relationship between these two species is thus completely equivalent to that of $(Cp_2TiCl)_2$ and Cp_2TiCl; i.e., the dimerization of Cp_2TiBr to $(Cp_2TiBr)_2$ is reversible, with the dimer having the lowest oxidation potential. In summary, we conclude that the reduction mechanism for Cp_2TiBr_2 can be encompassed in the scheme outlined for Cp_2TiCl_2.

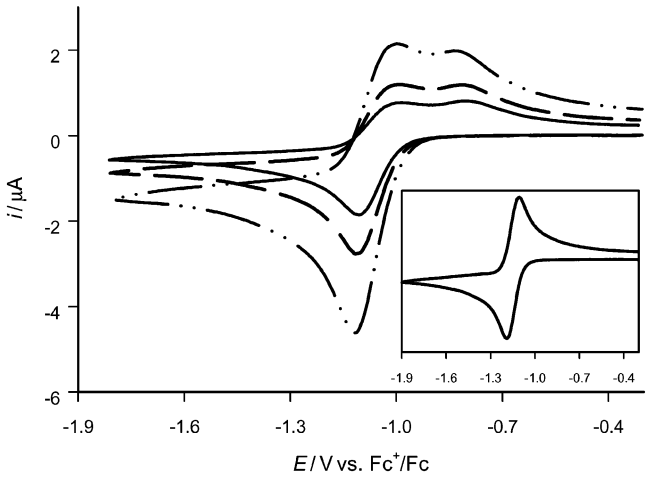

Figure 6. Cyclic voltammograms of Cp_2TiBr_2 in concentrations of 0.4 (—), 0.6 (– –), and 1.0 mM (– ·· –) recorded at a sweep rate of 1 V s^{-1} in 0.2 M Bu_4NPF_6/THF. Inset: cyclic voltammogram of 1 mM Cp_2TiBr_2 in the presence of 18 mM Bu_4NBr recorded at a sweep rate of 1 V s^{-1} in 0.2 M Bu_4NPF_6/THF.

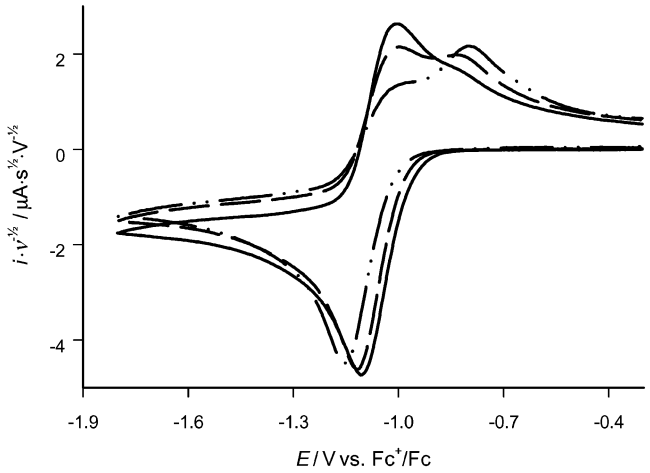

Figure 7. Cyclic voltammograms of 1 mM Cp_2TiBr_2 recorded at sweep rates of 0.1 (—), 1 (– –), and 10 V s^{-1} (– ·· –) in 0.2 M Bu_4NPF_6/THF. Currents are normalized with respect to sweep rate.

Cp_2TiI_2. Cyclic voltammograms of Cp_2TiI_2 recorded for different sweep rates and concentrations are collected in Figures 8 and 9. The overall appearance is as expected from the corresponding reduction of the two other titanocene dihalides, with the important note that the cleavage reaction in eq 2 is so favorable that the detection of $Cp_2TiI_2^-$ requires employment of even lower sweep rates, higher substrate concentrations, or the presence of Bu_4NI (see inset of Figure 8). For voltammograms recorded at low sweep rates, a small prewave is detectable, which we assign to the reduction of Cp_2TiI^+ formed by dissociation of Cp_2TiI_2. That such a dissociation should be observable for Cp_2TiI_2 and not

(33) Green, M. L. H.; Lucas, C. R. *J. Chem. Soc., Dalton Trans.* **1972**, 1000.

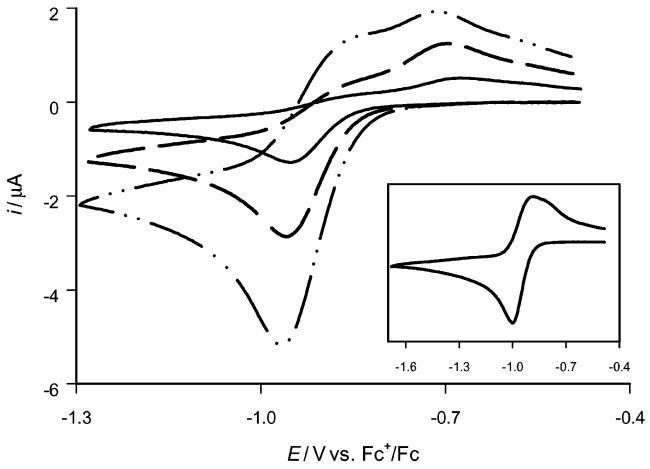

Figure 8. Cyclic voltammograms of Cp_2TiI_2 in concentrations of 0.3 (—), 0.6 (– –), and 1.1 mM (– •• –) recorded at a sweep rate of 1 V s^{-1} in 0.2 M Bu_4NPF_6/THF. Inset: Cyclic voltammogram of 1 mM Cp_2TiI_2 in the presence of 10 mM Bu_4NI recorded at a sweep rate of 1 V s^{-1} in 0.2 M Bu_4NPF_6/THF.

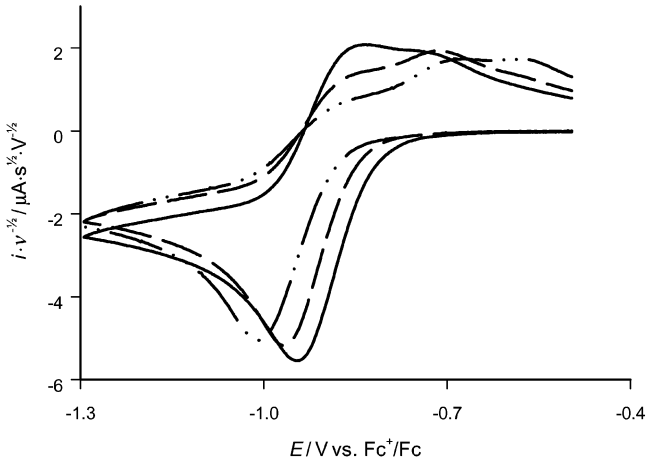

Figure 9. Cyclic voltammograms of 1.1 mM Cp_2TiI_2 recorded at sweep rates of 0.1 (—), 1 (– –), and 10 V s^{-1} (– •• –) in 0.2 M Bu_4NPF_6/THF. Currents are normalized with respect to sweep rate.

Cp_2TiBr_2 or Cp_2TiCl_2 is in line with the finding that a THF solution of Cp_2TiI_2 is the only one having a measurable conductivity and that the Ti—I bond is the weakest of the three Ti—halogen bonds.[34]

In summary, the complete reaction mechanism for the electrochemical reduction of Cp_2TiX_2 (X = Cl, Br, I) can be set up as shown in Scheme 1 (denoted a mesh scheme). The scheme is based on the assumption that Cp_2TiX with its free coordination site is the only Ti^{III}-based species reacting with X^- to produce $Cp_2TiX_2^-$. The reactivity of the $(Cp_2TiX)_2$ dimer toward X^- is expected to be lower, although it should be noted that its reactions with electrophiles can be quite fast, according to kinetic studies presented elsewhere.[31] The dissociation of Cp_2TiX_2 to Cp_2TiX^+ and X^- is important only in the case of X = I, as described above. The mesh scheme for "Cp_2TiCl", which is slightly different because of the inclusion of eqs 4, 5, and 8 rather than eqs 9 and 10, is available in the Supporting Information.

Scheme 1. Mesh Scheme Describing the Mechanism for the Electrochemical Reduction of Cp_2TiX_2

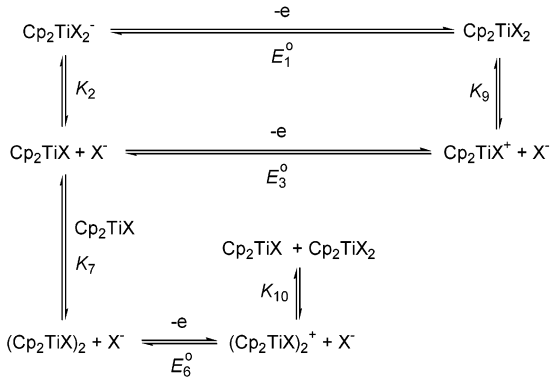

On the basis of the proposed mechanism, simulations of cyclic voltammograms have been carried out using the program DigiSim 3.03 in order to extract all relevant thermodynamic and kinetic parameters.[35] The adjustable parameters in the simulation procedure include standard potentials, equilibrium constants, homogeneous and heterogeneous rate constants, symmetry factors, and diffusion coefficients. Of these, the last two are considered to be of less importance and thus they are kept fixed. The values of the standard potentials, $E°$, and the heterogeneous rate constants, k_s, are very important for the quality of the fits, as they essentially determine the position of the peaks. For k_s we find relatively small values less than 0.1 cm s^{-1}: therefore, the electrode processes can be considered to be quasi-reversible for most of the sweep rates employed. Thus, the influence on the peak potentials from homogeneous follow-up or preceding reactions is not as pronounced as if the electrode processes had been reversible. On the other hand, the homogeneous kinetics in terms of the rate constants involved exerts a large influence on the peak currents and the wave pattern. The simulation program ensures that the parameters involved obey the fundamental thermodynamical laws: i.e., when three out of four parameters in a thermochemical cycle have been defined, the fourth is calculated automatically and cannot be altered independently of the others. All voltammograms are fitted simultaneously in order to obtain the most consistent set of data. Because of the many adjustable parameters present, it is important that the number of experimental observations be large. This is accomplished by varying the sweep rate (0.1—50 V s^{-1}), the substrate concentration (0.1—2.0 mM), and the concentration of Bu_4NX (0—18 mM). A detailed description of the exact model parameters used and a compilation of relevant fits can be found in the Supporting Information.

To illustrate some of the features, we have collected voltammograms recorded for Cp_2TiBr_2 at different sweep rates and concentrations of Cp_2TiBr_2 and Bu_4NBr in Figures 10—12 along with the best fits. The fact that the extent by which the oxidation proceeds through $Cp_2TiBr_2^-$ decreases upon increasing the sweep rate or lowering the concentration (see Figures 10 and 11) provides direct information about the rate constant

(34) *Handbook of Chemistry and Physics*, 72nd ed.; Lide, D. R., Ed.; CRC Press: Boca Raton, FL, 1991.

(35) Rudolph, M.; Feldberg, S. W. *DigiSim version 3.03;* Bioanalytical Systems, Inc.

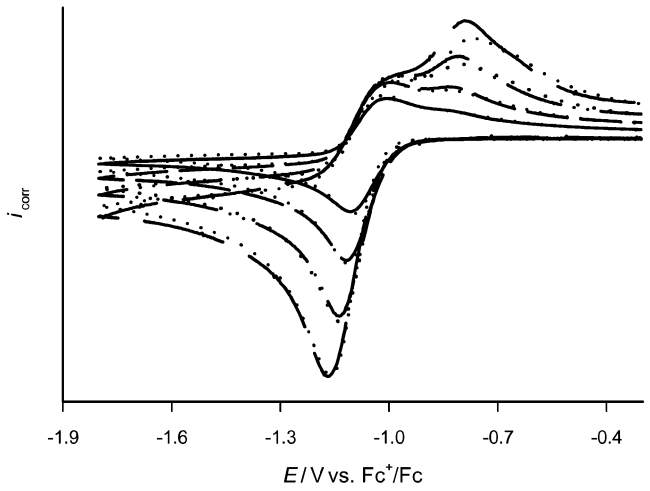

Figure 10. Recorded and simulated (dotted lines) cyclic voltammograms of 1 mM Cp_2TiBr_2 at sweep rates of 0.2 (—), 1 (– –), 5 (– ·· –), and 20 V s^{-1} (— —) in 0.2 M Bu_4NPF_6/THF. The currents i_{corr} are corrected arbitrarily to facilitate comparison. The simulation parameters employed can be found in Table 1 and in the Supporting Information.

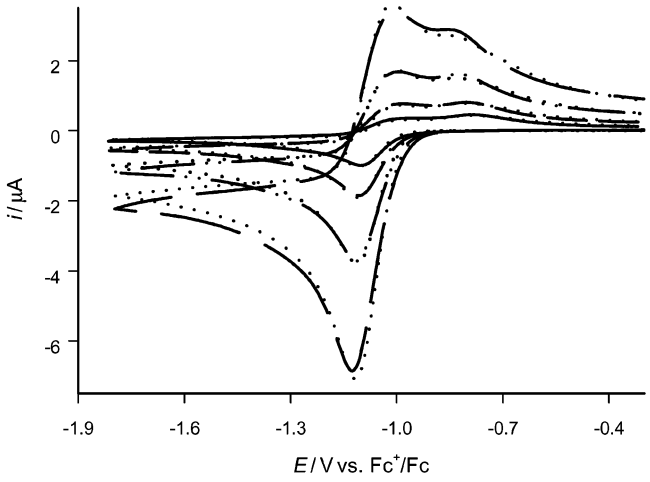

Figure 11. Recorded and simulated (dotted lines) cyclic voltammograms of Cp_2TiBr_2 in concentrations of 0.2 (—), 0.4 (– –), 0.8 (– ·· –), and 1.5 mM (— —) at a sweep rate of 1 V s^{-1} in 0.2 M Bu_4NPF_6/THF. The simulation parameters employed can be found in Table 1 and in the Supporting Information.

of back-association, k_{-2}. At the same time this behavior shows that the major part of the Ti^{III}-based species is on the form of either Cp_2TiBr or $(Cp_2TiBr)_2$ rather than $Cp_2TiBr_2^-$. Figure 12 illustrates the dramatic effect of adding Br^- as the oxidation wave of $Cp_2TiBr_2^-$ increases, because of the enhancement of the back-association reaction rate in eq 2. This effect also provides the reason that a relatively large shift in the peak potentials for the $Cp_2TiBr_2/Cp_2TiBr_2^-$ wave occurs.

The results extracted from the simulation of the cyclic voltammograms of Cp_2TiX_2 (X = Cl, Br, I) and "Cp_2TiCl", along with the estimated uncertainties, are collected in Table 1. Note that all potentials listed are referenced against Fc^+/Fc but that they can easily be converted to SCE by adding 0.52 V.[36] The parameters pertaining to eqs 5 and 8 are specifically related to the "Cp_2TiCl" case, and these results are available only in the Supporting Information. In general, the uncertainty associated with the measurements on the latter system is quite large, as the low stability of the solutions causes a poor reproducibility of the recorded cyclic voltammograms. In a forthcoming publication[31] we will show that essentially the same solutions but with a much larger stability can be generated through a metal reduction of Cp_2TiCl_2. While a detailed discussion of the "Cp_2TiCl" case therefore will be offered elsewhere,[31] it is still interesting at this point to compare the results with those extracted for the Cp_2TiCl_2 case because of the coincidence of species. As seen, the agreement between the data sets is acceptable, although deviations of 90−100 mV are found for the $E°_3$ and $E°_6$ parameters. Presumably this should be ascribed to the uncertainties associated with the characterization of the small waves recorded for Cp_2TiCl and $(Cp_2TiCl)_2$ in the cyclic voltammograms of Cp_2TiCl_2.

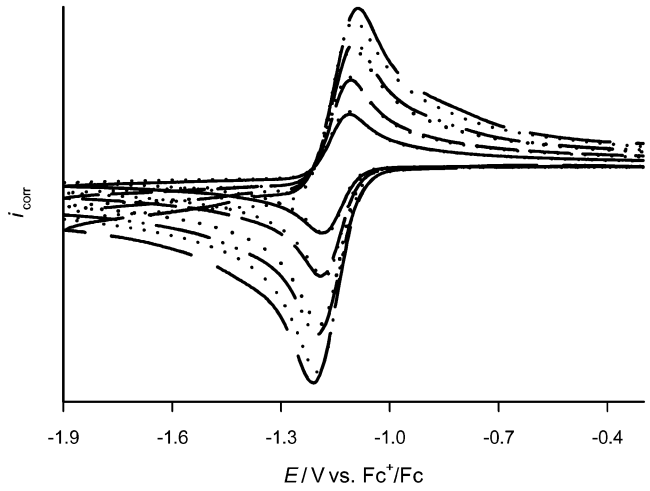

Figure 12. Recorded and simulated (dotted lines) cyclic voltammograms of 1 mM Cp_2TiBr_2 in the presence of 18 mM Bu_4NBr at sweep rates of 0.5 (—), 1 (– –), 5 (– ·· –), and 10 V s^{-1} (— —) in 0.2 M Bu_4NPF_6/THF. The currents i_{corr} are corrected arbitrarily to facilitate comparison. The simulation parameters employed can be found in Table 1 and in the Supporting Information.

Some general trends are apparent in the extracted parameters. For a given X the electron-donating abilities of the different Ti^{III}-based species, as judged from the standard potentials determined, are $Cp_2TiX_2^- \gg (Cp_2TiX)_2 > Cp_2TiX \gg Cp_2Ti^+$. For a given Ti^{III}-based species, the decrease in the standard potentials is in the order X = I, Br, Cl. The latter is expected on account of the higher polarizability of Br and, in particular, I which will make it easier to encompass the extra electron from an energetic point of view. At the same time the cleavage rate constants k_2 for $Cp_2TiX_2^-$ and k_{-9} for Cp_2TiX_2 decrease in the same halogen order, which is related to the concomitant increase in the strength of the Ti−X bond, going from 310 to 439 and 494 kJ mol^{-1} for X = I, Br, Cl, respectively.[34] The standard heterogeneous rate constants are all in the range of 0.008−0.08 cm s^{-1}.

On the basis of the extracted equilibrium constants it is possible to evaluate the equilibrium concentrations

(36) Enemærke, R. J.; Daasbjerg, K.; Skrydstrup, T. *Chem. Commun.* **1999**, 343.

Table 1. Relevant Data Extracted from Cyclic Voltammograms Recorded on Solutions Containing "Cp_2TiCl", Cp_2TiCl_2, Cp_2TiBr_2, and Cp_2TiI_2[a]

	"Cp_2TiCl"	Cp_2TiCl_2	Cp_2TiBr_2	Cp_2TiI_2
$E°_1$/V vs Fc^+/Fc[b]	−1.27 ± 0.04	−1.27 ± 0.02	−1.14 ± 0.02	−1.01 ± 0.02
$E°_6$/V vs Fc^+/Fc[b]	−0.81 ± 0.02	−0.90 ± 0.04	−0.84 ± 0.04	−0.74 ± 0.04
$E°_3$/V vs Fc^+/Fc[b]	−0.75 ± 0.01	−0.85 ± 0.04	−0.80 ± 0.04	−0.60 ± 0.04
$E°_4$/V vs Fc^+/Fc[b]	−0.41 ± 0.02			
$k_{s,1}$/cm s^{-1}	0.04	0.04	0.08	0.07
$k_{s,6}$/cm s^{-1}	0.02	0.02	0.08	0.06
$k_{s,3}$/cm s^{-1}	0.008	0.01	0.02	0.04
$k_{s,4}$/cm s^{-1}	0.015			
K_2/M		1 (0.5−2) × 10^{-4}	6.5 (5−8) × 10^{-3} [c]	5 (4−6) × 10^{-2} [c]
k_2/s^{-1}		2 (0.5−2) × 10^4	3 (2−5) × 10^4 [c]	2 (1−3) × 10^5 [c]
k_{-2}/M^{-1} s^{-1}		2 (1−2) × 10^8	4.6 (4−6) × 10^6 [c]	4 (2−6) × 10^6 [c]
K_7/M^{-1}	3 (2−7) × 10^3	5 (3−10) × 10^3	5 (3−10) × 10^3	5 (3−10) × 10^3
k_7/M^{-1} s^{-1}	2 (0.5−4) × 10^4	2 (1−10) × 10^5	5 (0.5−10) × 10^7	2 (1−10) × 10^5
k_{-7}/s^{-1}	6.7 (2−17)	40 (30−100)	1 (0.2−3) × 10^4	40 (10−300)
K_9/M^{-1} [d]		1.7 (0.5−10) × 10^{11}	1.1 (0.2−5) × 10^8	2.2 (1−10) × 10^8
k_9/M^{-1} s^{-1}		1 × 10^{10} [e]	5 (2−20) × 10^5 [f]	1 (0.01−100) × 10^8 [f]
k_{-9}/s^{-1}		6 × 10^{-2} [g]	4.7 (0.4−100) × 10^{-3}	0.45 (0.005−50)
K_{10} [d]		4.6 (0.4−40) × 10^6	4.4(1−20) × 10^3	1.7 (0.5−50) × 10^2
k_{10}/M^{-1} s^{-1}		1 × 10^{10} [e]	1 (0.1−10) × 10^8 [f]	1 (0.5−5) × 10^4 [f]
k_{-10}/M^{-1} s^{-1}		2.2 (0.3−25) × 10^3 [g]	2.3 (0.2−20) × 10^4	59 (30−300)

[a] The tabulated values are the ones providing the best fits, while those given in parentheses describe the intervals of tolerance, as determined from a manual adjustment of the parameters. To minimize the number of adjustable parameters, the uncertainties on the k_s values were not determined, but in general they can be assumed to be on the order of 50%. [b] Potentials can be converted to SCE by adding 0.52 V. [c] The oxidation wave pattern is quite sensitive toward changes in these values. [d] Calculated automatically from a thermochemical cycle. [e] The reaction rate is assumed to be close to the diffusion-controlled limit, although simulations show that the reduction wave pattern in double-sweep experiments is practically unaffected by the exact magnitude of the rate constant, as long as it is larger than 10^6 M^{-1} s^{-1}. [f] Determined from double-sweep experiments (see the Supporting Information). [g] Upper limit determined on the assumption that k_9 and $k_{10} = 10^{10}$ M^{-1} s^{-1}.

Table 2. Equilibrium Concentrations of the Ti^{III}-Based Species Present in a 2 mM Solution of Electrochemically Reduced Cp_2TiX_2 and in a 2 mM Solution of "Cp_2TiCl"[a]

	$[Cp_2TiX_2^-]$	$[Cp_2TiX]$	$[(Cp_2TiX)_2]$
X = Cl	1.35 (1.95)	0.21 (0.04)	0.22 (0.007)
X = Br	0.11 (0.36)	0.39 (0.36)	0.75 (0.64)
X = I	0.02 (0.05)	0.40 (0.39)	0.79 (0.78)
"Cp_2TiCl"	0 (1.92)	0.5 (0.06)	0.75 (0.01)

[a] The numbers in parentheses provide the corresponding distribution in the presence of 5 mM Bu_4NX. Concentrations are given in mM.

of $Cp_2TiX_2^-$, Cp_2TiX, and $(Cp_2TiX)_2$ upon an electrochemical one-electron reduction of Cp_2TiX_2. For a concentration of 2 mM we find the distribution listed in Table 2. From these data it is evident that while the major constituent is $Cp_2TiX_2^-$ in the case of X = Cl, Cp_2TiX and $(Cp_2TiX)_2$ are the main species for X = Br, I. As the concentration is increased, $(Cp_2TiX)_2$ and $Cp_2TiX_2^-$ will be favored at the expense of Cp_2TiX. The same will be true for solutions of "Cp_2TiCl", although in this case obviously no $Cp_2TiCl_2^-$ will be present. In the presence of 5 mM Bu_4NX the concentration of $Cp_2TiX_2^-$ becomes substantial also for X = Br but not X = I, as shown in Table 2.

To elucidate which of the Ti^{III}-based species formed in the electrochemically reduced solutions of Cp_2TiX_2 are the most reactive ones, a few kinetic measurements were carried out. Benzyl chloride was selected as electron acceptor, as its precoordination abilities were assumed to be small. Still, the reaction kinetics are quite complex, because $Cp_2TiX_2^-$, Cp_2TiX, and $(Cp_2TiX)_2$ will all be present together in the solutions. While a detailed description of the kinetics concerning the last two species can be found elsewhere,[31] we intend to deal with the role of $Cp_2TiX_2^-$ herein by examining the effect on the reaction kinetics of adding Bu_4NX to the solutions.

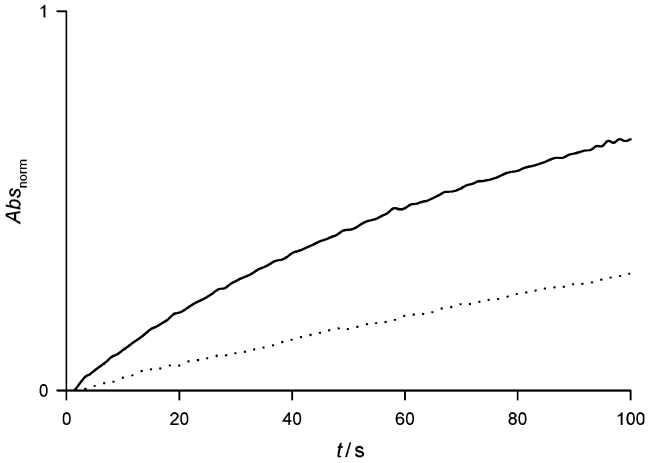

Figure 13. Kinetic traces recorded for the buildup of Ti^{IV} at λ 530 nm for the reaction between 87 mM benzyl chloride and a 2 mM electrochemically reduced solution of Cp_2TiCl_2 without (—) and in the presence of 5 mM Bu_4NCl (···). Absorbances have been normalized to facilitate comparison.

In particular, this is of interest in the case of X = Cl, as $Cp_2TiCl_2^-$ should be the major constituent according to the above analysis (see Table 2). The kinetics was followed by means of UV−vis spectroscopy, as discussed in the Experimental Section.

In Figures 13 and 14 kinetic traces pertaining to the buildup of Ti^{IV} in the reaction between electrochemically reduced solutions of Cp_2TiX_2 (X = Cl, Br, I) and benzyl chloride are collected. As seen, the reactivities for X = Br, I are comparable and somewhat larger than for X = Cl. At the same time, the effect of adding Bu_4NX is very much dependent on the nature of X; i.e., while the kinetics for X = Cl becomes substantially slower, there is a relatively small or no influence at all on the kinetics

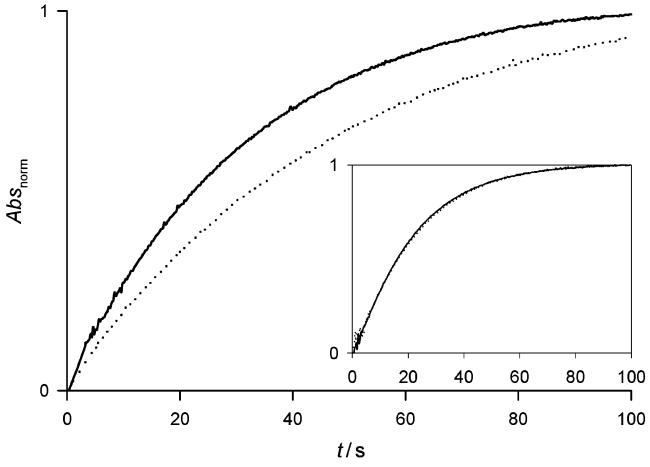

Figure 14. Kinetic traces recorded for the buildup of Ti^{IV} at λ 530 nm for the reaction between 87 mM benzyl chloride and a 2 mM electrochemically reduced solution of Cp_2TiBr_2 without (—) and in the presence of 5 mM Bu_4NBr (···). Inset: kinetic traces recorded for the buildup of Ti^{IV} at λ 530 nm for the reaction between 87 mM benzyl chloride and a 2 mM electrochemically reduced solution of Cp_2TiI_2 without (—) and in the presence of 5 mM Bu_4NI (···). Absorbances have been normalized to facilitate comparison.

for X = Br, I, respectively. This behavior is in line with the equilibrium distribution of $Cp_2TiX_2^-$ and $Cp_2TiX/(Cp_2TiX)_2$, in the sense that one goes from $Cp_2TiCl_2^-$ as the dominant species to have some $Cp_2TiBr_2^-$ and essentially no $Cp_2TiI_2^-$ in the presence of Bu_4NX (see Table 2). Thus, we may conclude that the reactive species in all solutions are Cp_2TiX and/or $(Cp_2TiX)_2$ rather than $Cp_2TiX_2^-$ and that the varying effects of Bu_4NX observed on the reaction kinetics can be explained by taking into account eq 2, the influence of which increases in the halogen order X = I, Br, and Cl. On this assumption and on the basis of rough exponential fits, we find that the upper limit of the rate constant for the reactions of $Cp_2TiCl_2^-$, $Cp_2TiBr_2^-$, and $Cp_2TiI_2^-$ with benzyl chloride can be set at 0.019, 0.12, and 0.26 M^{-1} s^{-1}, respectively. A discussion of these numbers along with those determined for the other Ti^{III}-based species will be provided elsewhere.[31]

In summary, we have shown that the electrochemical reduction of Cp_2TiX_2 leads mainly to the formation of $Cp_2TiX_2^-$ for X = Cl, whereas a mixture of Cp_2TiX and $(Cp_2TiX)_2$ is generated for X = Br, I. The presence of $(Cp_2TiX)_2$ in solution is surprising, as THF was believed to be capable of breaking the weak dimeric structure. The rate constants for cleavage of X^- from the different Ti^{III}-based species increase in the halogen order X = Cl, Br, I because of the concomitant decrease in the strength of the Ti—X bond. The Cp_2TiX and $(Cp_2TiX)_2$ species are found to be much more reactive than $Cp_2TiX_2^-$, although they were expected to be poorer electron donors, as judged from the standard potentials determined. Thus, it may be concluded that the prospects of generating reactive Ti^{III}-based species electrochemically seem most promising in the cases of Cp_2TiBr_2 and Cp_2TiI_2. In a forthcoming publication concerning the use of metals for carrying out reductions of Cp_2TiX_2, these aspects will be further discussed.[31]

Experimental Section

Chemicals. Most chemicals were of commercial origin unless otherwise noted. Tetrahydrofuran, THF, was distilled over sodium and benzophenone under an atmosphere of dry nitrogen. Argon (99.99% purity) was passed through a column of P_2O_5 (Sicapent) prior to use. Tetrabutylammonium hexafluorophosphate, Bu_4NPF_6, was prepared from a hot aqueous solution containing tetrabutylammonium hydrogen sulfate and potassium hexafluorophosphate. The precipitate was filtered and recrystallized from ethyl acetate and pentane. Tetrabutylammonium chloride, Bu_4NCl, was recrystallized twice using THF. The white crystals were dried under vacuum at 60 °C for 24 h and stored in a glovebox. All handling of Bu_4NCl had to occur under a dry atmosphere because of its hygroscopic properties. Tetrabutylammonium bromide, Bu_4NBr, and tetrabutylammonium iodide, Bu_4NI, were recrystallized and treated as described above for Bu_4NCl. Thallium hexafluorophosphate, $TlPF_6$, was dried under vacuum at 60 °C for 24 h. Thallium cyclopentandienide, TlCp, was sublimated under vacuum at 80 °C.[37] Bis(cyclopentadienyl)titanium dichloride, Cp_2TiCl_2, was recrystallized from toluene. Bis(cyclopentadienyl)titanium dibromide, Cp_2TiBr_2, was prepared by adding 1.1 mL of a 1.0 M BBr_3/CH_2Cl_2 solution to 250 mg of Cp_2TiCl_2 (1 mmol) dissolved in 10 mL of CH_2Cl_2. After 15 min of stirring the solution was evaporated. The red-brown residue was dissolved in 20 mL of CH_2Cl_2, and after filtration this solution was evaporated as well. The product was dried under vacuum for 3—4 h at room temperature.[38] Bis(cyclopentadienyl)titanium diiodide, Cp_2TiI_2, was synthesized using the same procedure as described for Cp_2TiBr_2, with BBr_3 replaced by BI_3. The solution of "Cp_2TiCl" was prepared as described in ref 10. Typically, 23 mg of $TiCl_3$ (0.15 mmol) was suspended in 5 mL of THF and added to a solution of 81 mg of TlCp (0.30 mmol) in 1.5 mL of THF. While the solution was refluxed for 15 min, it turned green and a precipitation of TlCl occurred. The separation was carried out using syringe techniques. The concentration was determined from peak current measurements.

Apparatus. In cyclic voltammetry a standard three-electrode setup was employed with a glassy-carbon electrode (diameter 1 mm, Sigradur) serving as working electrode. The latter was polished on a special cloth using a 0.25 μm diamond abrasive (Struers A/S), washed with ethanol, and air-dried before it was mounted in the cell. The reference electrode employed was Ag/AgI ($[I^-] = 0.1$ M). At the same time the Fc^+/Fc redox couple was used as internal reference, the potential of which is 0.52 V vs SCE.[36] A platinum coil served as counter electrode. The ohmic drop was compensated with a positive feedback system incorporated in the home-built potentiostat. The kinetic traces were recorded by means of a fiber-optic spectrometer, Model S1000 (dip-probe), from Ocean Optics.

Procedure. In the cyclic voltammetric experiments 0.77 g of Bu_4NPF_6 (2 mmol) and a small magnetic bar were added to the electrochemical cell. The cell was closed and flushed thoroughly with argon for 10 min. Typically 9 mL of freshly distilled THF and 1 mL of the appropriate standard solution containing the compound of interest were added to the cell using a syringe, and the solution was stirred for 30 s. For Cp_2TiI_2 we did note, however, that the solution was relatively unstable and another procedure was chosen, in which solid Cp_2TiI_2 was placed directly in the cell along with Bu_4NPF_6 prior to the addition of THF. A fresh solution was prepared for each sample of Cp_2TiI_2, the concentration of which could be determined from the recorded peak currents. At the end of each series of experiments a small amount of ferrocene was added and the potential of the Fc^+/Fc couple was measured.

(37) Nielson, A. J.; Rickard, C. E. F.; Smith, J. M. *Inorg. Synth.* **1990**, *28*, 315.
(38) Druce, P. M.; Kingston, B. M.; Lappert, M. F.; Spalding, T. R.; Srivastava, R. C. *J. Chem. Soc. A* **1969**, 2106.

In the kinetic experiments the UV−vis dip probe was mounted vertically in a two-necked cell containing a small magnetic bar. The cell was closed and flushed with argon for 10 min before 9 mL of freshly distilled THF was added. From a standard solution of electrogenerated $Cp_2TiX_2^-$ typically 1 mL was transferred to the cell. Benzyl chloride was added in large excess while the solution was stirred vigorously. The decay of Ti^{III} at λ 800 nm as well as the buildup of Ti^{IV} at λ 530 nm were followed simultaneously. The kinetics followed the rate law: $-d[Ti^{III}\ \text{species}]/dt = d[Ti^{IV}\ \text{species}]/dt = 2k[Ti^{III}\ \text{species}][\text{benzyl chloride}]$.

Supporting Information Available: Text giving a description of the model parameters used in the simulations and figures giving a compilation of relevant fits. This material is available free of charge via the Internet at http://pubs.acs.org.

OM034360H